Science of the Total Environment 754 (2021) 142394

Contents lists available at ScienceDirect

Science of the Total Environment

journal homepage: www.elsevier.com/locate/scitotenv

Quantifying the anthropogenic and meteorological influences on summertime surface ozone in China over 2012–2017

Ruijun Dang [a], Hong Liao [b,*], Yu Fu [c]

[a] State Key Laboratory of Atmospheric Boundary Layer Physics and Atmospheric Chemistry (LAPC), Institute of Atmospheric Physics, Chinese Academy of Sciences, Beijing 100029, China
[b] Jiangsu Key Laboratory of Atmospheric Environment Monitoring and Pollution Control, Jiangsu Collaborative Innovation Center of Atmospheric Environment and Equipment Technology, School of Environmental Science and Engineering, Nanjing University of Information Science and Technology, Nanjing 210044, China
[c] Climate Change Research Center, Chinese Academy of sciences, Beijing 100029, China

HIGHLIGHTS

- Both anthropogenic and meteorological factors favored recent ozone increases in NCP and YRD.
- In NCP, higher temperature, regional transport, and enhanced natural emissions were major meteorological drivers.
- In YRD, weaker wind speed and lower humidity are major meteorological drivers.
- Extreme ozone increasing trends are more meteorology-induced than average conditions.

GRAPHICAL ABSTRACT

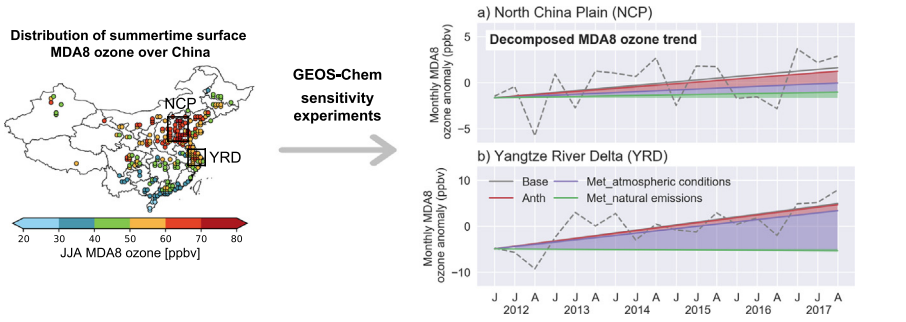

ARTICLE INFO

Article history:
Received 25 July 2020
Received in revised form 11 September 2020
Accepted 12 September 2020
Available online 18 September 2020

Editor: Jianmin Chen

Keywords:
Ozone trend
Anthropogenic emissions
Meteorology
Natural emissions

ABSTRACT

We applied the global 3-D chemical transport model GEOS-Chem to examine the anthropogenic and meteorological contributions in driving summertime (JJA) surface ozone (O_3) trend in China during the Clean Air Action period 2012–2017. The model captures the observed spatial distribution of summertime O_3 concentrations in China ($R = 0.78$) and reproduces the observed increasing trends in two most populated city clusters: North China Plain (NCP) and Yangtze River Delta (YRD). Trend of simulated maximum daily 8-h average (MDA8) O_3 concentration is 0.58 ppbv yr^{-1} in NCP and 1.74 ppbv yr^{-1} in YRD in JJA 2012–2017. Sensitivity studies show that both changes in anthropogenic emissions and meteorology favored the MDA8 O_3 increases in these two regions with respective contributions of 39% and 49% in NCP, and 13% and 84% in YRD. In NCP, the 49% meteorology impact includes a considerable contribution from natural emissions (19%). Changes in biogenic VOCs, soil NO_x, and lightning NO_x emissions are estimated to enhance MDA8 O_3 in NCP with a rate of 0.14, 0.10, and 0.14 ppbv yr^{-1}, respectively. In YRD, natural emissions made small contributions to the MDA8 O_3 trend. Statistical analysis shows that higher temperatures and anomalous southerlies at 850 hPa in 2017 relative to 2012 are the two major meteorological drivers in NCP that favored the O_3 increases, while weaker wind speed and lower relative humidity are those for YRD. We further examined the trend of fourth highest daily maximum 8-h average (4MDA8) O_3 among a specific month that linked with extreme pollution episodes. Trends of simulated 4MDA8 O_3 in NCP and YRD are 34–46% higher than those of MDA8 O_3 and are found more meteorology-induced. Our results suggest an important role of meteorology in driving summertime O_3 increases in China in recent years.

* Corresponding author.
E-mail address: hongliao@nuist.edu.cn (H. Liao).

https://doi.org/10.1016/j.scitotenv.2020.142394
0048-9697/

1. Introduction

Stringent Clean Air Action was initiated in 2013 by Chinese government, aiming to improve $PM_{2.5}$ air quality by 2017. However, whilst $PM_{2.5}$ concentrations decreased drastically, ozone (O_3) pollution is getting worse during the period, especially in the rapidly developed regions such as the North China Plain (NCP) and the Yangtze River Delta (YRD) (Dang and Liao, 2019, K Li et al., 2019, Shen et al., 2019). From 2013 to 2017, observed warm-season (April–September) mean maximum daily 8-h average (MDA8) O_3 concentrations increased at a rate of 3% yr^{-1} for 74 key cities over China (Lu et al., 2018), and the 90th percentile of MDA8 O_3 evidently increased from 65 ppbv in 2013 to 78 ppbv in 2017 (Fu et al., 2019). Exposure to high concentrations of O_3 is detrimental to human health (Cohen et al., 2017) and to vegetation growth (Yue et al., 2017). Therefore, elucidating the increasing trend of O_3 in China is critical for development of air pollution control strategies.

Surface O_3 is a secondary pollutant produced by photochemical oxidation of volatile organic compounds (VOCs) and carbon monoxide (CO) in the presence of nitrogen oxides ($NO_x = NO+NO_2$). These O_3 precursors are intensively emitted from anthropogenic sources and some natural sources such as VOCs from vegetation and NO_x from soil and lightning. Sensitivity of O_3 production is nonlinearly dependent on precursor concentrations, and can be categorized into photochemical regimes such as NO_x-limited or VOC-limited (Kleinman, 1994; Sillman, 1999). In VOC-limited regime, for example, reduction in VOCs emissions can result in decreases in O_3 concentrations, but NO_x reduction has a weak effect or even opposite. O_3 formation in polluted urban areas is generally reported as VOC-limited, while that in rural areas falls in NO_x-limited or transitional regime (Jin and Holloway, 2015, T Wang et al., 2017, Xue et al., 2014).

In addition to emissions, variations of O_3 are highly sensitive to changes in meteorology. Hot, dry, stagnant conditions are often associated with high O_3 events, as these days typically favor the formation and persistence of O_3 (Gong and Liao, 2019; Han et al., 2020). Increased local O_3 levels can also be linked with long-range/regional transport of pollutant air (Gao et al., 2020; Ni et al., 2018; Yang et al., 2014), or with suppression of dry depostion in extremely hot days (Lu et al., 2019). Besides factors mentioned above, meteorology can influence O_3 levels through affecting natural emissions. Increases in ambient temperature can accelerate the emission rate of biogenic VOCs and soil NO_x, and these two sources are also influenced by soil moisture, light, and vegetation type (Jacob and Winner, 2009; Porter and Heald, 2019). NO_x from lightning is influenced by parameters related to deep convection (Ott et al., 2010).

Several studies have investigated the drivers of O_3 increases in China in the past few years. By using a regional chemical transport model, N Wang et al. (2019) found that 30% NO_x reductions in 2012 could lead to 3.0–8.3% increment in O_3 levels in megacity clusters (eg. NCP, YRD) where the formation of O_3 is VOC-limited. In work of K Li et al. (2019), they examined individual anthropogenic factor (including NO_x/VOCs emission changes, $PM_{2.5}$ changes) in driving June–August 2013–2017 O_3 trend in China, and $PM_{2.5}$ reduction was reported as the dominant anthropogenic driver because the decreases of $PM_{2.5}$ led to a slowdown of HO_2 uptake and thus accelerated the O_3 production. By taking advantage of GEOS-Chem model, Lu et al. (2019) explored the sources of May–August O_3 in China over 2016–2017, and they found that the O_3 increases in 2017 relative to 2016 were mainly caused by enhancement of natural sources of soil NO_x and biogenic VOC, as a result of hotter and drier meteorological conditions in 2017. These studies show that rapid reductions in anthropogenic emissions during the Clean Air Action period could result in O_3 increases in China, and changes in meteorology could also play important roles. However, little is known yet about meteorological influences on O_3 trend over 2012–2017, and so is the contrast between meteorological impact and emission impact.

In this study, our aim is to better understand the underlying factors that facilitated the summertime (June–July-August) O_3 increases in China during 2012–2017, not only separating anthropogenic and meteorological influences, but further exploring contributions from individual natural emission changes and quantifying the relative importance of each meteorological variable. We interpret the increasing trends of O_3 using a global 3-D chemical transport model GEOS-Chem together with a statistical model. We focus not only on the trends of MDA8 O_3, but also on those of fourth highest daily maximum 8-h average (4MDA8) O_3.

2. Methods

2.1. Surface O_3 monitoring network

Hourly surface O_3 observations are obtained from the China National Environmental Monitoring Center (CNEMC) (http://www.cnemc.cn/en/). This network starts with 496 sites (in 74 major cities) in 2013 and quickly expanded to nationwide 1597 sites (in 454 cities) by 2017. We use the 2013–2017 observations to evaluate the model's performance in simulating summertime surface O_3. Quality controls are implemented to remove unreliable measurements based on Lu et al. (2018), and for each site, only the days with valid data more than 16 h a day are reserved. Overall, we select 408 sites in 2013 and 713 continuous sites for 2014–2017 that have sufficient measurements for more than 80% availability each JJA. We average the site-monitored data on the 0.5° latitude x 0.625° longitude model grid for model evaluation.

2.2. Model description

We simulate concentrations of O_3 using the nested-grid version (0.5° latitude by 0.625° longitude over Asia 11°S-55°N, 60–150°E) of the GEOS-Chem model (version 11–01; http://acmg.seas.harvard.edu/geos/) driven by MERRA-2 meteorological fields (Gelaro et al., 2017). The model includes fully coupled HO_x-NO_x-VOC-O_3-aerosol chemistry, with approximate 300 chemical species participated in over 400 kinetic and photolysis reactions (Bey et al., 2001; Mao et al., 2013; Park et al., 2004). Photolysis rates are calculated based on Fast-JXv7.0 scheme (Eastham et al., 2014). Dry deposition follows a standard resistance-in-series model (Wesely, 1989), with multiple modifications from Y H Wang et al. (1998).

Global anthropogenic emissions are from the Community Emissions Data System (CEDS) (Hoesly et al., 2018), overwritten by year-specific Multi-resolution Emission Inventory for China (MEIC) (Zheng et al., 2018) over China and MIX inventory (M Li et al., 2017) over other regions of East Asia. Natural emissions are calculated online based on MERRA-2 meteorology. Soil NO_x emissions are computed using an updated version of the Berkeley-Dalhousie Soil NO_x Parameterization (BDSNP) scheme (Hudman et al., 2012). Lightning NO_x emissions are treated using the parameterization based on cloud top height (Price and Rind, 1992) and are further constrained by climatological data from the Lightning Imaging Sensor (LIS) and the Optical Transient Detector (OTD) satellite observations (Murray et al., 2012). Biogenic emissions of VOCs are calculated following the Model of Emissions of Gases and Aerosols from Nature (MEGANv2.1) as described in Guenther et al. (2012).

Fig. 1 shows the emission difference in summertime O_3 precursors in China between 2012 and 2017. As a result of clean air actions, anthropogenic emissions of CO and NO_x decreased over most China, with largest reductions found in NCP and YRD. Anthropogenic VOCs increased over eastern China, except for Hebei, Shandong, and Shanxi provinces. This increment of anthropogenic VOCs emissions is reported due to the growth in solvent use and the absence of effective emission control measures in this period (Zheng et al., 2018). VOCs from vegetation and NO_x from soil are strongly temperature dependent, and their changes therefore spatially followed that of daily maximum 2-m temperature (T-2 m) in 2017 with respect to 2012 (Fig. S1). The T-2 m increases spread over northern China and some eastern coastal areas, while decreases are found in southern provinces. Column-integrated

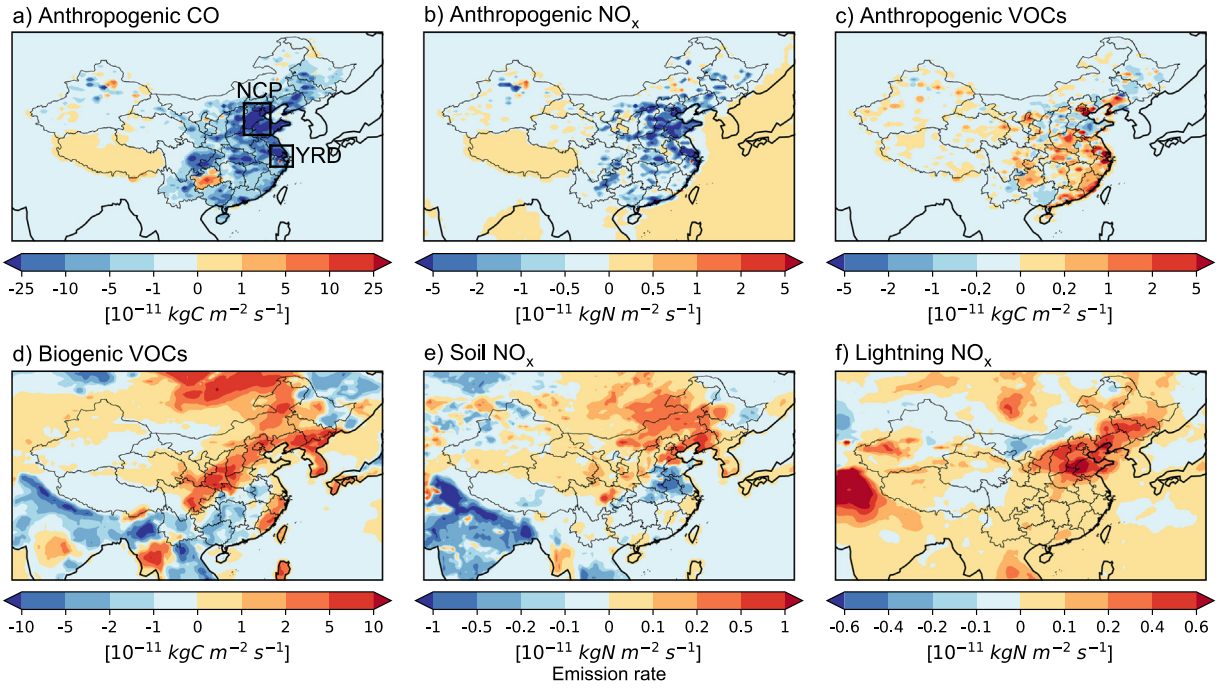

Fig. 1. Emission changes in summertime (JJA) mean **a)** anthropogenic CO, **b)** anthropogenic NO_x, **c)** anthropogenic VOCs, **d)** biogenic VOCs, **e)** soil NO, and **f)** lightning NO_x between 2012 and 2017 (2017 minus 2012). Polygons in the topleft panel define the regions of the North China Plain (NCP: 35–41° N, 113.75–118.75° E) and the Yangtze River Delta (YRD: 29–33° N, 118.75–123° E). Note that for lightning NO_x, the emission rate is column integrated.

lightning NO_x shows widespread increases over eastern China, with largest changes occurred in NCP and northeast China. Emissions over NCP and YRD are summarized in Table 1.

2.3. Numerical experiments

To investigate the relative importance of individual anthropogenic/meteorological factors in affecting the overall trend of surface O_3 in China during JJA 2012–2017, we conduct multiple sensitivity simulations with the GEOS-Chem model (Table 2). The standard simulation (Base) includes variations of both anthropogenic emissions and meteorological fields over 2012–2017. In sensitivity simulations, we only allow the variations in anthropogenic emissions (Anth)/meteorological fields (Met) over 2012–2017 whilst fix the meteorological fields /anthropogenic emissions in 2012 conditions. O_3 variations in Anth simulation therefore represent the impact of changes in anthropogenic emissions, and those in Met simulation represent the impact of changes in all meteorology-related processes.

In Met simulation, meteorology can affect O_3 variations through influencing chemical reactions, transport, and depositions of pollutants, and through influencing natural emissions of O_3 precursors. To isolate the impact of natural emissions, we further conducted a simulation by fixing natural emissions (including biogenic VOCs, soil NO_x, and lightning NO_x) at 2012 levels (Met_atm) as compared to Met simulation. O_3 variations in Met_atm simulation therefore represent the impact of changes in atmospheric conditions alone. Effects of natural emission changes are then estimated as the difference between Met and Met_atm simulation.

Three additional sensitivity simulations are performed to identify the impact of individual natural emission source. Based on configurations in Met simulation, we further fix natural emissions of (1) biogenic VOCs (Met_noBiog), (2) soil NO_x (Met_noSoil), and (3) lightning NO_x (Met_noLight) at 2012 levels individually. Contribution from each natural source can therefore be identified as the difference between the Met simulation and each sensitivity simulation.

Table 1
Summertime (JJA) emissions from anthropogenic and natural sources over regions of North China Plain (NCP) and Yangtze River Delta (YRD).

Emissions		NCP			YRD		
		2012	2017	Change	2012	2017	Change
Anthropogenic CO	(Tg C)	3.32	2.19	−34.1%	1.39	1.03	−25.8%
Anthropogenic NO_x	(Tg N)	0.43	0.31	−28.3%	0.24	0.18	−23.7%
Anthropogenic VOCs	(Tg C)	0.54	0.56	+2.2%	0.43	0.47	+10.2%
Biogenic VOCs	(Tg C)	0.29	0.34	+17.3%	0.29	0.30	+4.4%
Soil NO_x	(Tg N)	0.042	0.044	+4.9%	0.008	0.007	−15.6%
Lightning NO_x	(Tg N)	0.019	0.033	+73.3%	0.006	0.007	+14.5%

3. Results and discussion

3.1. Simulated O_3 in China over 2012–2017 and model evaluation

Fig. S2 evaluates the simulation for 2014–2017 with the summertime mean MDA8 O_3 observations for the same period. The model reproduces the spatial distribution of observed surface MDA8 O_3 with high spatial correlation coefficient R of 0.78. Observed high O_3 spots in NCP and YRD (>60 ppbv) are well captured by the simulation. Observed and modeled MDA8 O_3 concentrations average 53.1 ± 11.3 and 68.3 ± 11.2 ppbv (mean ± standard deviation), respectively, for the sites in Fig. S2. The overestimations at urban sites in our model (normalized mean bias NMB = 28.6%) are also reported in other modeling works using GEOS-Chem (Lu et al., 2019; Ni et al., 2018), and were largely attributed to the deficiencies in representing small-scale emissions, rapid chemical conversions, and complex meteorological conditions in urban areas in the model (Sun et al., 2019; Young et al., 2018).

Fig. 2 shows the simulated monthly mean MDA8 O_3 trend for JJA 2012–2017 in the two regions highlighted in Fig. 1: NCP and YRD. The trends are calculated based on O_3 anomalies by substracting 2012–2017 means for individual summer month. Also shown is the observed O_3 anomaly trend for 2013–2017 when measurements are available. Comparisons between observed and simulated trends over

Table 2
Configurations of GEOS-Chem simulations in this study.

Simulation	Anthropogenic emissions	Meteorological fields	Biogenic VOC emissions	Soil NO_x emissions	Lightning NO_x emissions
Base	2012–2017	2012–2017	2012–2017	2012–2017	2012–2017
Anth	2012–2017	2012	2012	2012	2012
Met	2012	2012–2017	2012–2017	2012–2017	2012–2017
Met_atm	2012	2012–2017	2012	2012	2012
Met_noBiog	2012	2012–2017	2012	2012–2017	2012–2017
Met_noSoil	2012	2012–2017	2012–2017	2012	2012–2017
Met_noLight	2012	2012–2017	2012–2017	2012–2017	2012

2013–2017 show that the model well captures the increasing tendencies of summertime surface MDA8 O_3 in NCP and YRD, but underestimates the observed trend, especially in NCP. Observed and simulated MDA8 O_3 trend in 2013–2017 is 1.82 and 0.45 ppbv yr^{-1}, respectively, for NCP, and 1.63 and 1.16 ppbv yr^{-1}, respectively, for YRD. The underestimated trend in NCP is partly due to the model's deficiencies in capturing the extreme O_3 pollution episodes in the summer of 2017 (especially June), as suggested by Fig. S3. Such under predictions of peak values of O_3 are also reported in other modeling works using GEOS-Chem (Gong and Liao, 2019; Lu et al., 2019; Ni et al., 2018) and regional models such as CMAQ or WRF-Chem (Chen et al., 2018; Gao et al., 2020). Many factors may contribute to the under predictions of O_3 extremes, such as the missing of vegetation feedbacks on O_3 concentrations in the model (Lin et al., 2020), the missing of nitrous acid (HONO) sources (Tie et al., 2019; Zhang et al., 2019), and the representative issues of emissions, meteorology, and chemistry in the model due to the coarse resolution (Young et al., 2018 and references therein).This underestimation of observed O_3 trend is also reported by K Li et al. (2019) and they speculated that was related to coarse spatial resolution (50-km) in the GEOS-Chem model, thus unable to capture the strongly VOC-limited conditions in urban areas. For 2012–2017 period, simulated MDA8 O_3 shows an increasing trend of 0.58 ppbv yr^{-1} in NCP and 1.74 ppbv yr^{-1} in YRD.

3.2. Anthropogenic vs. meteorological contribution to MDA8 O_3 trends in 2012–2017

Fig. 3 explores the effects of changes in anthropogenic emissions and meteorology on the 2012–2017 MDA8 O_3 trends. In the BASE simulation, simulated MDA8 O_3 increased in NCP, YRD, and western China, and decreased in southwest China, northeast China, and Xinjiang province. Simulated trends are in range of 0–1 ppbv yr^{-1} in NCP and 1–3 ppbv yr^{-1} in YRD. Changes in anthropogenic emissions (Fig. 1a-c) are simulated to lead to MDA8 O_3 increases in urban areas of NCP, YRD, and the Pearl River Delta (0–1 ppbv yr^{-1}), while decreases elsewhere. This pattern is consistent with the expected distribution of VOC-limited and NO_x-limited conditions in China as suggested by previous studies (Jin and Holloway, 2015, T Wang et al., 2017). Changes in meteorology are found more important than anthropogenic emission changes in dominating the spatial variation and magnitude of MDA8 O_3 trends in the BASE simulation. The patterns in our study (Fig. 3a-c) are consistent with those in work of Liu and Wang (2020a) (Fig. 2), who conducted similar simulations for 2013–2017 MDA8 O_3 concentrations in China by using a regional model WRF-CMAQ.

We next separate the overall meteorological impacts into: effect of changes in atmospheric conditions (referred to as atmospheric effect), and effect of changes in natural emissions (referred to as natural emission effect). The pattern of simulated 2012–2017 MDA8 O_3 trends resulting from atmospheric effect alone (Fig. 3d) is in good agreement with the pattern from the combined impacts of atmospheric conditions and natural emissions (Fig. 3c) and therefore identified as the main driver as compared to natural emission effect (Fig. 3e). Changes in natural emissions are estimated to elevate summertime surface MDA8 O_3 in northern and southeastern China, but decrease O_3 levels in central China such as Jiangsu, Anhui, Hunan, and Hubei provinces. Simulated 2012–2017 MDA8 O_3 trends from natural emission changes range from −0.5 to 0.5 ppbv yr^{-1} over China.

Contributions of individual natural emission source to the MDA8 O_3 trends are further identified in Fig. 3f-h. The patterns of simulated MDA8 O_3 trends from biogenic VOCs and soil NO_x changes roughly follow the patterns of emission changes themselves (Fig. 1d-e), but with slight inconsistencies found between them. These inconsistencies are possibly due to the varied sensitivity of O_3 formation to NO_x/VOCs changes, or the transport impact on precursor distributions. The largest biogenic VOCs impacts are spatially centered in NCP, Shanxi, and Shannxi provinces, with contributions in range of 0.1–0.4 ppbv yr^{-1}. Trends from soil NO_x changes are highest over Inner Mongolia, with values in range of 0.1–0.5 ppbv yr^{-1}. Although lightning NO_x enhancement mainly distributed at upper troposphere around 300 hPa, stronger subsidence in 2017 relative to 2012 has brought the upper-formed O_3 down to the ground and enhanced the surface O_3 (Fig. S4). Lightning NO_x effect is largest over the Tibet Plateau (0.4–0.7 ppbv yr-^{1}) due to the high elevation. In eastern China, lightning NO_x changes have a larger impact in the northern areas (0.1–0.4 ppbv yr^{-1}) than in the southern areas (0–0.1 ppbv yr^{-1}).

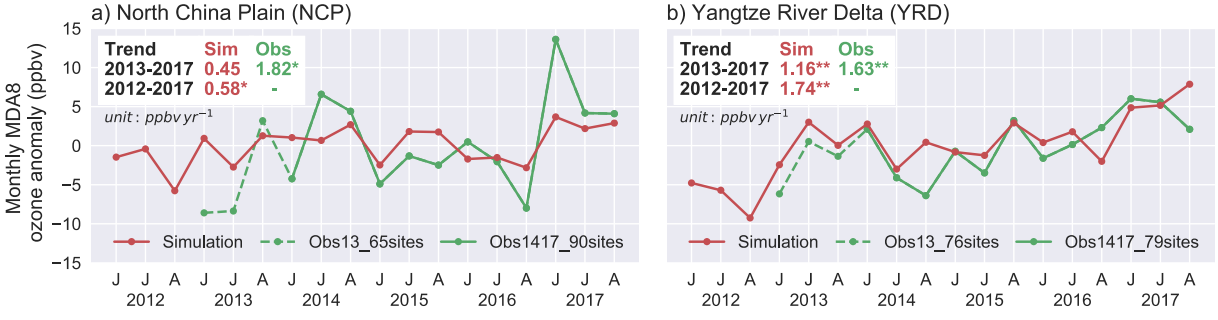

Fig. 2. Time series of monthly mean MDA8 O_3 anomalies (unit: ppbv) in summer (JJA) 2012–2017 for the two highlighted regions of Fig. 1: NCP and YRD. MDA8 O_3 values are averaged for each region and month, and anomalies are calculated relative to the 2012–2017 means for that month of the year. Lines in red/green represent the results from GEOS-Chem simulations/CNEMC observations. Values inset in each panel are linear regression trends (unit: ppbv yr^{-1}), and those marked with ** and * are statistically significant at 0.05 and 0.1 level, respectively. (For interpretation of the references to colour in this figure legend, the reader is referred to the web version of this article.)

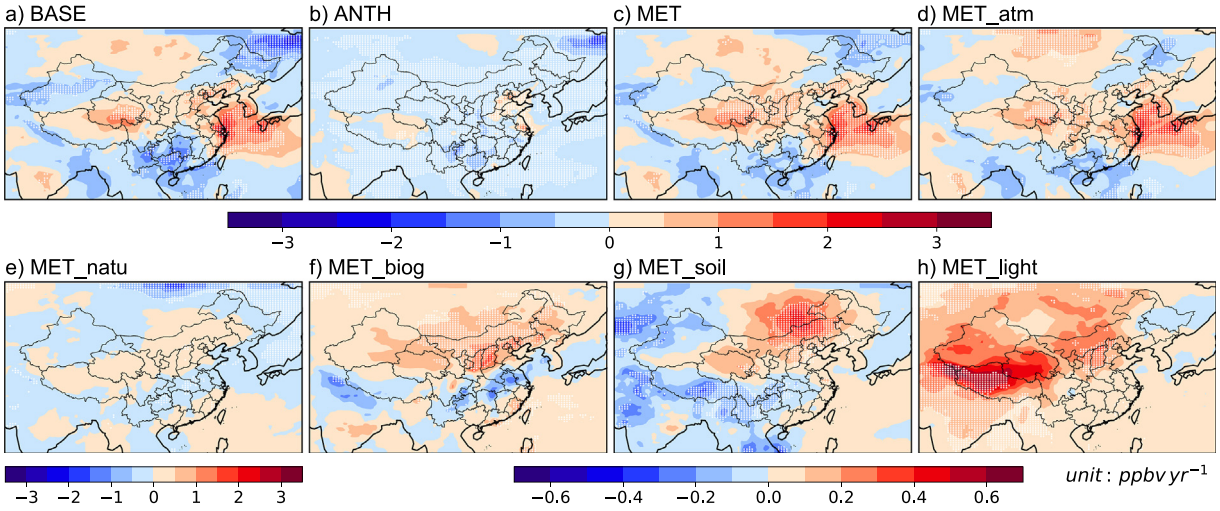

Fig. 3. Trends of simulated JJA MDA8 O_3 concentrations in China (unit: ppbv yr^{-1}) driven by changes in a) anthropogenic emissions and meteorology, b) anthropogenic emissions, c) meteorology, d) atmospheric conditions, e) natural emissions, f) biogenic VOCs emissions, g) soil NO_x emissions, and h) lightning NO_x emissions over 2012–2017. See Table 2 for detailed experimental design. Trends that are statistically significant above 90% confidence level are marked with dots.

We now focus on two most populated city clusters: NCP and YRD and investigate the contribution of individual anthropogenic and meteorological driver on regional 2012–2017 MDA8 O_3 trends (Fig. 4a-b).

3.2.1. NCP

Simulated MDA8 O_3 in NCP has an increasing trend of 0.58 ppbv yr^{-1} over 2012–2017, with combined changes in anthropogenic emissions and meteorology. Both changes in anthropogenic emissions and meteorology favored O_3 increases in NCP, with comparable contributions of 0.23 ppbv yr^{-1} (39%) and 0.28 ppbv yr^{-1} (49%), respectively. Note that the sum of 0.23 and 0.28 is unequal to 0.58 because of the nonlinear relationship between the simulations. For the 49% part resulting from meteorological changes, atmospheric effect alone is estimated to lead to a trend of 0.18 ppbv yr^{-1} (30%) for MDA8 O_3, and natural emission changes further facilitated the increase with a contribution of 0.11 ppbv yr^{-1} (19%). Simulated 2012–2017 MDA8 O_3 trends resulting from changes in biogenic VOCs, soil NO_x, and lightning NO_x is 0.14, 0.10, and 0.14 ppbv yr^{-1}, respectively, in NCP. It should be noted that the total impact of separate natural source is not equivalent to the impact of total natural sources, which is mainly due to the nonlinear relationship between O_3 concentration and its precursors.

3.2.2. YRD

Simulated 2012–2017 MDA8 O_3 trend is 1.74 ppbv yr^{-1} in YRD in the BASE simulation. Similar to NCP, changes in anthropogenic emissions and meteorology jointly facilitated the increases of MDA8 O_3 in YRD, while the different thing is that in YRD, meteorological impacts contributed a larger share of 1.47 ppbv yr^{-1} (84%). Anthropogenic emission changes alone are estimated to lead to a MDA8 O_3 trend of 0.23 ppbv yr^{-1} (13%). The 1.47 ppbv yr^{-1} MDA8 O_3 trend from both changes in atmospheric conditions and natural emissions is mostly contributed by the atmospheric effect (1.54 ppbv yr^{-1}, 89%) that far offset the negative effect brought by natural emission changes (−0.07 ppbv yr^{-1}, −4%). Changes in individual natural source show small contributions to the overall trend of MDA8 O_3 in YRD over 2012–2017.

Our result is similar to those by Liu and Wang (2020a) for Beijing (in NCP) and Shanghai (in YRD) between 2013 and 2017, both suggesting positive roles of anthropogenic emissions and meteorology in driving recent O_3 increases. On the other hand, our result differs from theirs that reflects a considerable contribution of meteorological changes to O_3 increasing trends in NCP and YRD. Many factors might cause the result differences, such as the scale we concerned (regional or city scale), the treat of boundary conditions in simulations (global or regional model), or the selected period.

3.3. Comparisons between MDA8 and 4MDA8 O_3 trends

Previous study pointed out that at Chinese sites between 2013 and 2017, metrics that focus on high O_3 concentrations (e.g. 4MDA8) exhibited more evident increases, as compared to average conditions (Lu et al., 2018). Therefore in this section, we further investigate the trends of 4MDA8 O_3 in China over 2012–2017 and explore the underlying factors that led to faster increases of 4MDA8 O_3 in comparison with monthly mean MDA8 O_3. Here, we define 4MDA8 O_3 as the 4th highest MDA8 O_3 concentration in a month (approximately 90th percentile), which represents the high end of O_3 distribution and is likely related to extreme pollution episodes.

Fig. 5 examines the effects of changes in anthropogenic emissions and meteorology on the 2012–2017 4MDA8 O_3 trend. Simulated 4MDA8 O_3 trends in BASE, ANTH, and MET simulation generally follow the patterns of MDA8 O_3 trends in Fig. 3 but having larger magnitudes. Trends of 4MDA8 O_3 from BASE simulation range from 0 to 2 ppbv yr^{-1} in NCP and from 1 to 5 ppbv yr^{-1} in YRD, indicating a faster growth rate in tail of O_3 distribution. Like that in MDA8 O_3, the spatial pattern of 4MDA8 O_3 trends in BASE simulation (Fig. 5a) is largely defined by meteorological effects over 2012–2017 (Fig. 5c), other than changes in anthropogenic emissions. One obvious difference is found in natural emissions effect. Other than showing non-uniform contribution in eastern China for MDA8 O_3 trends, changes in natural emissions are estimated to lead to widespread 4MDA8 O_3 increases in eastern China during 2012–2017, with resulted trends in range of 0–1 ppbv yr^{-1}. Of the three natural emission sources, changes in biogenic VOCs emissions are found mostly responsible for this spatial difference between Figs. 3e and 5e. Contributions of biogenic emissions are estimated to range from 0.2 to 0.8 ppbv yr^{-1} in eastern China for 4MDA8 O_3 trends, much higher than those of −0.3 to 0.4 ppbv yr^{-1} in the same area for MDA8 O_3. Enhanced biogenic contributions is likely associated with the larger and broader increases in extreme temperature values over eastern China between 2012 and 2017 (Fig. S5). Results on regions of NCP and YRD (Fig. 6) are discussed below.

3.3.1. NCP

Considering both changes in anthropogenic emissions and meteorology, trend of simulated 4MDA8 O_3 in NCP is 0.78 ppbv yr^{-1} over

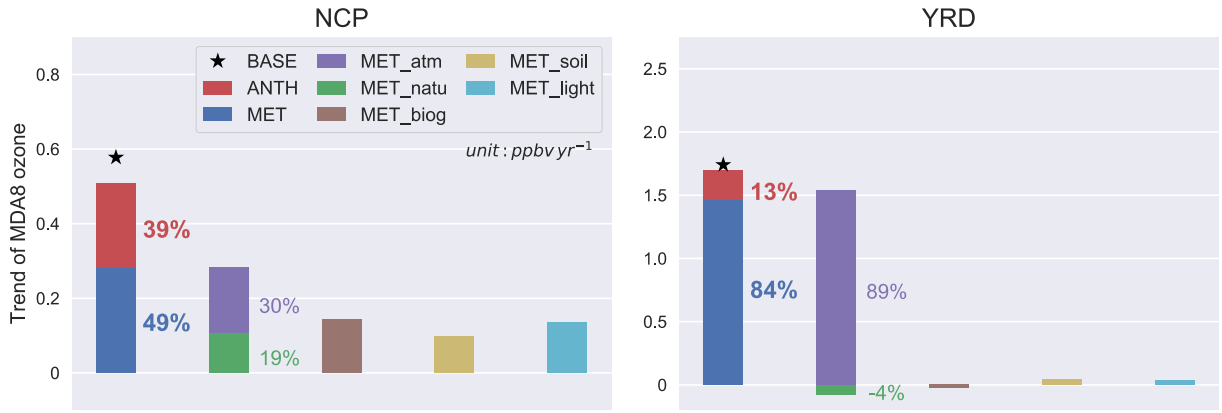

Fig. 4. Trends of simulated MDA8 O_3 concentrations in summertime (JJA) 2012–2017 for the two highlighted regions of Fig. 1 (unit: ppbv yr^{-1}). Decomposed O_3 trends resulting from individual driver in Fig. 3 is presented in colored bars. Values inset each panel are percentage contributions of each driver to the overall O_3 trends in the BASE simulation (marked as black star).

2012–2017, 34% larger than the trend of MDA8 O_3. This increasing trend of 4MDA8 O_3 is largely contributed by meteorological changes (0.60 ppbv yr^{-1}, 76%), and is further enhanced by anthropogenic emission changes (0.18 ppbv yr^{-1}, 22%). Of the 76% contribution from combined changes in atmospheric conditions and natural emissions, natural emission changes played a dominate role of 0.50 ppbv yr^{-1} (65%). Model results suggest that biogenic VOCs is the most important natural emission driver than soil and lightning NO_x in facilitating the larger 2012–2017 4MDA8 O_3 trend in NCP. Simulated 4MDA8 O_3 trend from biogenic emission changes is 0.34 ppbv yr^{-1}, more than twice the trend for MDA8 O_3. Impacts of soil and lightning NO_x changes on 4MDA8 O_3 trend are 0.11 and 0.19 ppbv yr^{-1}, respectively, showing small increases as compared to MDA8 O_3. Results from Ma et al. (2019) also highlighted the role of enhanced biogenic emissions during severe O_3 pollutions in NCP in the summer of 2017.

3.3.2. YRD

Simulated 4MDA8 O_3 in YRD exhibited a trend of 2.54 ppbv yr^{-1} in 2012–2017 in the BASE simulation, about 46% larger than that of MDA8 O_3. Changes in meteorology dominated the 4MDA8 O_3 increases in YRD with a contribution of 2.18 ppbv yr^{-1} (86%). Evident increase is found in natural emission contribution from −4% for MDA8 O_3 to 7% for 4MDA8 O_3 trend. Of the three natural emission sources, biogenic VOCs is identified as the most important natural emission driver with a contribution of 0.21 ppbv yr^{-1}.

To sum up, we find larger increasing trends in 4MDA8 O_3 in NCP and YRD during JJA 2012–2017 than in MDA8 O_3 on the basis of model results. When compared to MDA8 O_3, trends of 4MDA8 O_3 are more meteorology-induced, indicating a high dependency of extreme O_3 pollution episodes on conducive meteorological conditions (eg. extremely high temperature, persistent transport, weak ventilation). Additionally, natural emission changes are playing a more important role in 4MDA8 O_3 trends than in MDA8 O_3 trends, mainly due to the high sensitivity of vegetation emissions (eg. isoprene, monoterpenes) to hot and dry weather conditions. The above results suggest that more strict emission controls are required for limiting extreme O_3 values due to the coherence with unfavorable meteorological conditions.

3.4. Relative contribution of each meteorological parameter

So far we have discussed the impact of anthropogenic and meteorological changes on recent O_3 trends by taking advantage of modeling simulation, and the results indicate a significant role of meteorology. However, it is hard to examine the key meteorological parameter in this process by using chemical transport model. Here we apply a

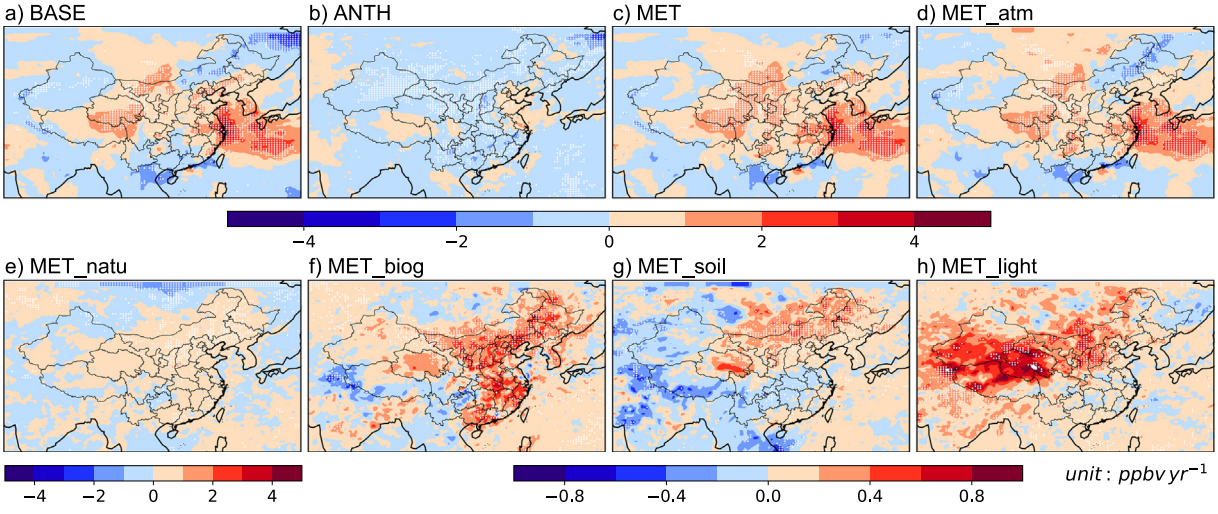

Fig. 5. Same as Fig. 3 except for 4MDA8 O_3 trends.

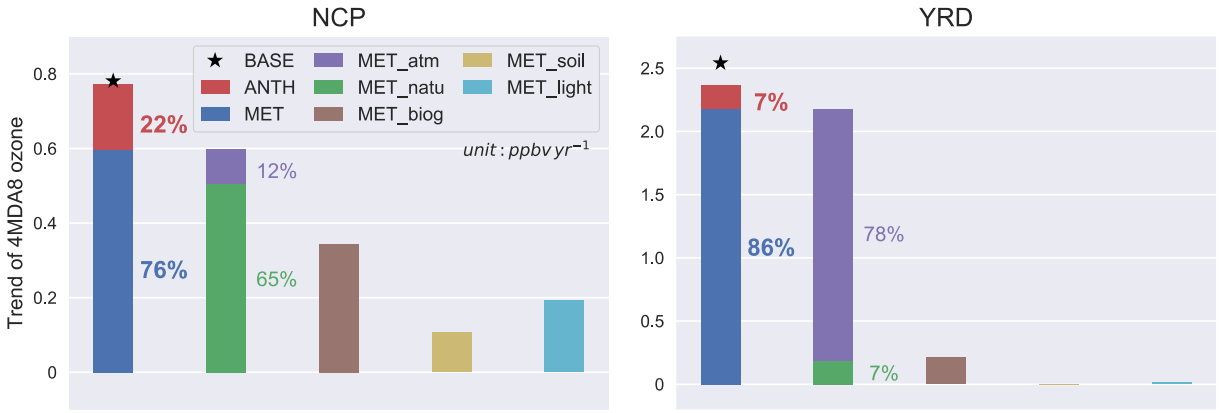

Fig. 6. Same as Fig. 4 except for 4MDA8 O_3 trends.

statistical model to quantify the relative importance of each meteorological parameter in the atmospheric effect.

We apply stepwise multiple linear regression (MLR) model for daily MDA8 O_3 concentrations in NCP and YRD from the Met_atm simulation, by considering a number of candidate meteorological variables from the MERRA-2 reanalysis. The MLR model is in the following form:

$$y = \beta_0 + \sum_{k=1}^{8} \beta_k x_k + interaction\ terms$$

where y is the daily MDA8 O_3 concentrations, and $(x_1,\ldots,x_8)$ are the eight meteorological variables (Table S1) that selected by a stepwise method featuring the best model fit (Han et al., 2020; Tai et al., 2010). All data for y and x_k are normalized for use by substracting 2012–2017 means for that day of the year and dividing by standard deviation. The coefficients of determination (R^2) for the MLR model in fitting MDA8 O_3 anomalies in NCP and YRD are 0.49 and 0.57, respectively, and are all statistically significant at 0.01 level. The MLR estimated regression coefficients β_k are summarized in Table S1.

We next use the LMG (Lindeman, Merenda, and Gold) method (Groemping, 2006) to quantify the relative importance of each of the eight meteorological variables in explaining the atmosphere-driven O_3 increases in NCP and YRD in 2012–2017. The LMG method can partition the MLR model-explained total R^2 into non-negative individual R^2 contribution from each correlated regressor. This approach has been used in many previous studies in examining the relative importance of model predictors in variations of $PM_{2.5}$ concentrations (Yang et al., 2016a), clouds and radiative forcing (Xu et al., 2015; Yang et al., 2016b). Fig. 7 shows the LMG decomposed contribution of eight meteorological variables (Table S1) in fitting MDA8 O_3 variations in NCP and YRD from the Met_atm simulation.

3.4.1. NCP

Increases in 2-m temperature (Fig. 8a) between 2012 and 2017 is the top driver for O_3 increases in NCP with a contribution of 31%. Hotter conditions can accelerate the chemical production of O_3 and thermal decomposition of peroxyacetyl nitrate (PAN), and the latter process can provide additional NO_x to produce O_3 (Doherty et al., 2013; Porter and Heald, 2019; Zhang et al., 2015). Followed that is the meridional wind at 850 hPa (NS) with a contribution of 30%. The positive regression coefficient for NS predictor (Table S1) and the southerly anomalies between 2012 and 2017 (Fig. 8b) together indicate a favourable role of southerly regional transport to the enhancement of local O_3 concentrations in NCP. Other thermodynamic meteorological parameters including lower relative humidity, lower cloud fraction, and less precipitation all indicate a dryer condition in 2017 relative to 2012, which altogether accounted for 27% contribution.

3.4.2. YRD

In YRD, the increases of O_3 is mostly driven by decreases in 10-m wind speed (WSPD, Fig. 8c) with a contribution up to 40%. Weaker wind speed can lead to less outflow of O_3 and its precursors to the downwind areas and end with more pollutants holding in YRD. Followed that is relative humidity (RH, 29%) and zonal wind (EW, 13%). Decreasing humidity (Fig. 8b) can be linked with lower cloud fraction and stronger solar radiation, therefore enhance the photochemical production of O_3 (Pu et al., 2017). The positive regression coefficient for EW predictor indicates a positive impact of westerly pollutant transport to the 2012–2017 O_3 increases in YRD. Overall, our results show that the atmosphere-driven O_3 increase in YRD is more contributed by wind field changes (WSPD+NS + EW + UP, about 60%), while that in NCP is more determined by thermodynamic field changes (T2M + RH + CLD + PREC, about 60%).

4. Conclusions

In this study, we explored the underlying factors contributing to 2012–2017 trends in summertime (June–July-August) surface O_3 in China by taking advantage of the GEOS-Chem model. We show that the model captures the spatial distribution of summertime mean O_3 concentrations ($R = 0.78$), and reproduces the observed increasing trends in two target megacity clusters: North China Plain (NCP) and Yangtze River Delta (YRD) fairly well.

Multiple sensitivity studies were conducted to quantify the respective impact of 2012–2017 changes in anthropogenic emissions and meteorology on the overall trend of O_3. Meteorological impact is further separated into atmospheric effect and natural emission effect, with individual natural source contribution identified. Additionally, stepwise MLR model together with a LMG method were used to examine the relative importance of each meteorological parameter in the atmospheric effect.

In NCP in the baseline simulation, simulated maximum daily 8-h average (MDA8) O_3 concentration shows a trend of 0.58 ppbv yr^{-1} during JJA 2012–2017. Both changes in anthropogenic emssions and meteorology favored the O_3 increase in NCP with comparable contribution of 39% and 49%, respectively. The meteorology impact includes a considerable contribution from natural emission effect (19%). Of the three natural sources, biogenic VOCs and soil NO_x enhanced MDA8 O_3 in NCP by 0.14 and 0.10 ppbv yr^{-1}, mainly driven by higher temperatures in 2017 relative to 2012; lightning NO_x elevated surface MDA8 O_3 with a trend of 0.14 ppbv yr^{-1}, due to larger lightning emissions between 2012 and 2017 and favourable vertical transport. Further analysing the atmospheric effect, we find that the increases in 2-m temperature and southerly anomalies at lower troposphere are two main meteorological drivers for O_3 enhancement in NCP.

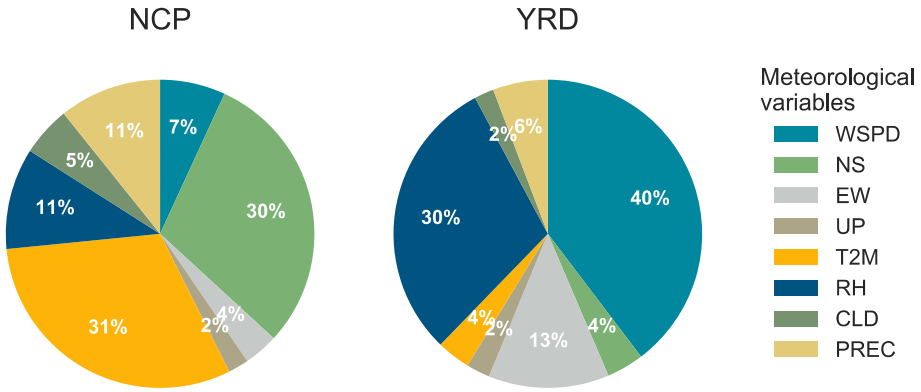

Fig. 7. The LMG method estimated relative importance (unit: %) of each meteorological variable in explaining the 2012–2017 variation of simulated summertime surface MDA8 O_3 concentrations over NCP and YRD from the Met_atm simulation. Predictors selected in MLR are wind speed at 10 m (WSPD), north-south direction indicator sin θ at 850 hPa (NS), east-west direction indicator cos θ at 850 hPa (EW), vertical pressure velocity at 850 hPa (UP), daily maximum 2-m temperature (T2M), relative humidity (RH), total cloud area fraction (CLD), and total precipitation (PREC).

In YRD in the baseline simulation, simulated MDA8 O_3 concentration increased at a rate of 1.74 ppbv yr^{-1} in JJA 2012–2017. Changes in meteorology dominated the MDA8 O_3 increases in YRD with a contribution of 84%, followed by anthropogenic emissions (13%). Natural emissions made small contribution to MDA8 O_3 trend in YRD. The LMG method suggested that weaker wind speed and lower relative humidity in 2017 relative to 2012 are two leading factors in explaining the atmosphere-driven MDA8 O_3 variations in YRD.

We further explored the trend of fourth highest daily maximum 8-h average (4MDA8) O_3 in JJA 2012–2017, which is linked with extreme pollution episodes. Simulated 4MDA8 O_3 trends in NCP and YRD are 34–46% larger than those of MDA8 O_3, and are more meteorology-induced when compared to MDA8 O_3 analysis. Natural emission changes played a more important role in 4MDA8 O_3 trends than in MDA8 O_3 trends, with contributions rose to 65% in NCP, and to 7% in YRD. The larger impact of natural emissions is found contributed by enhanced biogenic VOCs emissions under hotter conditions during severe O_3 pollutions. These results reflect a high dependency of extreme O_3 pollution episodes on conducive weather conditions such as extremely high temperature, persistent transport, and weak ventilation.

In conclusion, our results suggest that besides the anthropogenic drivers as revealed by previous studies (K Li et al., 2019, Liu and Wang, 2020b), meteorological conditions also played favourable roles in driving recent summertime O_3 increases in NCP and YRD, China, particularly for extreme O_3 pollutions. This poses a challenge for O_3 control, as more chances of extremely high temperatures in the future under climate change. Therefore, more strict and effective emission controls are required to counteract the meteorological impact in the upcoming 14th Five-Year Plan of China. Our results also highlight the significant role of biogenic VOCs emissions in O_3 increases, which indicates the necessity of controls on anthropogenic VOCs sources during the warm seasons.

CRediT authorship contribution statement

Ruijun Dang: Investigation, Formal analysis, Visualization, Writing - original draft. **Hong Liao:** Conceptualization, Supervision, Funding acquisition, Writing - review & editing. **Yu Fu:** Funding acquisition, Writing - review & editing.

Declaration of competing interest

The authors declare that they have no known competing financial interests or personal relationships that could have appeared to influence the work reported in this paper.

Acknowledgements

This work was supported by National Natural Science Foundation of China (grant no. 91744311) and the National Key Research and Development Program of China (grant no. 2019YFA0606804). F.Y. is supported by National Natural Science Foundation of China (grant no. 41977191). We appreciate the efforts from the GEOS-Chem working groups for developing and managing the model.

Data availability

All of the measurements, reanalysis data, and GEOS-Chem model code are publicly available from the websites given below. Hourly surface O3 observations are available from the public website of the China National Environmental Monitoring Center: http://www.cnemc.cn/en/. The MERRA-2 reanalysis meteorological data is openly accessible through https://gmao.gsfc.nasa.gov/reanalysis/MERRA-2/. The

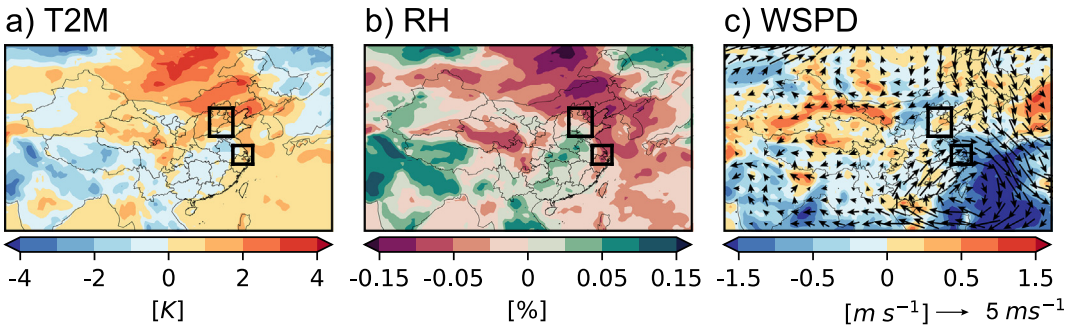

Fig. 8. Difference distributions of summertime (JJA) meteorological variables used in MLR model for 2017 with respect to 2012. Variables shown here are a) daily maximum 2-m temperature (T2M), b) relative humidity (RH), and c) 10-m wind speed (WSPD) with 850 hPa wind vectors over plotted. Polygons in each panel indicate regions of NCP and YRD.

GEOS-Chem model code can be downloaded from http://acmg.seas.harvard.edu/geos/.

Appendix A. Supplementary data

Supplementary data to this article can be found online at https://doi.org/10.1016/j.scitotenv.2020.142394.

References

Bey I et al 2001 Global modeling of tropospheric chemistry with assimilated meteorology: Model description and evaluation J. Geophys. Res.-Atmos. 106 23073–95.

Chen, X.Y., Liu, Y.M., Lai, A.Q., Han, S.S., Fan, Q., Wang, X.M., Ling, Z.H., Huang, F.X., Fan, S.J., 2018. Factors dominating 3-dimensional ozone distribution tropospheric ozone period environ. Pollut. 232, 55–64.

Cohen, A.J., et al., 2017. Estimates and 25-year trends of the global burden of disease attributable to ambient air pollution: an analysis of data from the Global Burden of Diseases Study 2015. Lancet 389, 1907–1918.

Dang, R., Liao, H., 2019. Radiative forcing and health impact of aerosols and ozone in China as the consequence of clean air actions over 2012–2017. Geophys. Res. Lett. 46, 12511–12519.

Doherty R M et al 2013 Impacts of climate change on surface ozone and intercontinental ozone pollution: A multi-model study Journal of Geophysical Research: Atmospheres 118 3744–63.

Eastham, S.D., Weisenstein, D.K., Barrett, S.R.H., 2014. Development and evaluation of the unified tropospheric-stratospheric chemistry extension (UCX) for the global chemistry-transport model GEOS-Chem Atmos. Environ. 89, 52–63.

Fu, Y., Liao, H., Yang, Y., 2019. Interannual and Decadal Changes in Tropospheric Ozone in China and the Associated Chemistry-Climate Interactions: A Review Advances in Atmospheric Sciences 36, 975–993.

Gao, M., et al., 2020. Ozone pollution over China and India: seasonality and sources. Atmos. Chem. Phys. 20, 4399–4414.

Gelaro, R., et al., 2017. The modern-era retrospective analysis for research and applications, version 2 (MERRA-2) J. Clim. 30, 5419–5454.

Gong, C., Liao, H., 2019. A typical weather pattern for ozone pollution events in North China Atmos. Chem. Phys. 19, 13725–13740.

Groemping U 2006 Relative importance for linear regression in R: the package relaimpo 2006 17 27.

Guenther A B, Jiang X, Heald C L, Sakulyanontvittaya T, Duhl T, Emmons L K and Wang X 2012 The Model of Emissions of Gases and Aerosols from Nature version 2.1 (MEGAN2.1): an extended and updated framework for modeling biogenic emissions Geosci. Model Dev. 5 1471–92.

Han, H., Liu, J., Shu, L., Wang, T., Yuan, H., 2020. Local and synoptic meteorological influences on daily variability in summertime surface ozone in eastern China Atmos. Chem. Phys. 20, 203–222.

Hoesly R M et al 2018 Historical (1750–2014) anthropogenic emissions of reactive gases and aerosols from the Community Emissions Data System (CEDS) Geosci. Model Dev. 11 369–408.

Hudman R C, Moore N E, Mebust A K, Martin R V, Russell A R, Valin L C and Cohen R C 2012 Steps towards a mechanistic model of global soil nitric oxide emissions: implementation and space based-constraints Atmospheric Chemistry and Physics 12 7779–95.

Jacob, D.J., Winner, D.A., 2009. Effect of climate change on air quality Atmos. Environ. 43, 51–63.

Jin X and Holloway T 2015 Spatial and temporal variability of ozone sensitivity over China observed from the Ozone Monitoring Instrument: Ozone Sensitivity over China Journal of Geophysical Research Atmospheres 120 7229–46.

Kleinman L I 1994 Low and high NOx tropospheric photochemistry Journal of Geophysical Research Atmospheres 991 16831–8.

Li M et al 2017 MIX: a mosaic Asian anthropogenic emission inventory under the international collaboration framework of the MICS-Asia and HTAP Atmospheric Chemistry and Physics 17 935-63.

Li, K., Jacob, D.J., Liao, H., Shen, L., Zhang, Q., Bates, K.H., 2019. Anthropogenic drivers of 2013-2017 trends in summer surface ozone in China Proc. Natl. Acad. Sci. U. S. A. 116, 422–427.

Lin M Y et al 2020 Vegetation feedbacks during drought exacerbate ozone air pollution extremes in Europe Nature Climate Change 10 444−+.

Liu, Y., Wang, T., 2020a. Worsening urban ozone pollution in China from 2013 to 2017-part 1: the complex and varying roles of meteorology. Atmos. Chem. Phys. 20, 6305–6321.

Liu, Y., Wang, T., 2020b. Worsening urban ozone pollution in China from 2013 to 2017-part 2: the effects of emission changes and implications for multi-pollutant control. Atmos. Chem. Phys. 20, 6323–6337.

Lu, X., et al., 2018. Severe surface ozone pollution in China: a global perspective Environ. Sci. Technol. Lett. 5, 487–494.

Lu, X., et al., 2019. Exploring 2016–2017 surface ozone pollution over China: source contributions and meteorological influences Atmos. Chem. Phys. 19, 8339–8361.

Ma, M., et al., 2019. Substantial ozone enhancement over the North China Plain from increased biogenic emissions due to heat waves and land cover in summer 2017 Atmos. Chem. Phys. 19, 12195–12207.

Mao J Q et al 2013 Ozone and organic nitrates over the eastern United States: Sensitivity to isoprene chemistry J. Geophys. Res.-Atmos. 118 11256–68.

Murray, L.T., Jacob, D.J., Logan, J.A., Hudman, R.C., Koshak, W.J., 2012. Optimized regional and interannual variability of lightning in a global chemical transport model constrained by LIS/OTD satellite data J. Geophys. Res.-Atmos. 117, 14.

Ni R J, Lin J T, Yan Y Y and Lin W L 2018 Foreign and domestic contributions to springtime ozone over China Atmospheric Chemistry and Physics 18 11447–69.

Ott L E, Pickering K E, Stenchikov G L, Allen D J, DeCaria A J, Ridley B, Lin R F, Lang S and Tao W K 2010 Production of lightning NOx and its vertical distribution calculated from three-dimensional cloud-scale chemical transport model simulations J. Geophys. Res.-Atmos. 115 19.

Park, R.J., Jacob, D.J., Field, B.D., Yantosca, R.M., Chin, M., 2004. Natural and transboundary pollution influences on sulfate-nitrate-ammonium aerosols in the United States: Implications for policy J. Geophys. Res.-Atmos. 109, 20.

Porter, W.C., Heald, C.L., 2019. The mechanisms and meteorological drivers of the summertime ozone–temperature relationship Atmos. Chem. Phys. 19, 13367–13381.

Price C and Rind D 1992 A SIMPLE LIGHTNING PARAMETERIZATION FOR CALCULATING GLOBAL LIGHTNING DISTRIBUTIONS J. Geophys. Res.-Atmos. 97 9919–33.

Pu X, Wang T J, Huang X, Melas D, Zanis P, Papanastasiou D K and Poupkou A 2017 Enhanced surface ozone during the heat wave of 2013 in Yangtze River Delta region, China Sci. Total Environ. 603-604 807-16.

Shen, L., Jacob, D.J., Liu, X., Huang, G., Li, K., Liao, H., Wang, T., 2019. An evaluation of the ability of the Ozone Monitoring Instrument (OMI) to observe boundary layer ozone pollution across China: application to 2005–2017 ozone trends Atmos. Chem. Phys. 19, 6551–6560.

Sillman, S., 1999. The relation between ozone, NOx and hydrocarbons in urban and polluted rural environments Atmos. Environ. 33, 1821–1845.

Sun, L., et al., 2019. Impacts of meteorology and emissions on summertime surface ozone increases over central eastern China between 2003 and 2015. Atmos. Chem. Phys. 19, 1455–1469.

Tai, A.P.K., Mickley, L.J., Jacob, D.J., 2010. Correlations between fine particulate matter (PM2.5) and meteorological variables in the United States: implications for the sensitivity of PM2.5 to climate change Atmos. Environ. 44, 3976–3984.

Tie X X, Long X, Li G H, Zhao S Y, Cao J J and Xu J M 2019 Ozone enhancement due to the photodissociation of nitrous acid in eastern China Atmospheric Chemistry and Physics 19 11267–78.

Wang Y H, Jacob D J and Logan J A 1998 Global simulation of tropospheric O-3-NOx-hydrocarbon chemistry 1. Model formulation J. Geophys. Res.-Atmos. 103 10713–25.

Wang T, Xue L K, Brimblecombe P, Lam Y F, Li L and Zhang L 2017 Ozone pollution in China: A review of concentrations, meteorological influences, chemical precursors, and effects Sci. Total Environ. 575 1582–96.

Wang, N., Lyu, X., Deng, X., Huang, X., Jiang, F., Ding, A., 2019. Aggravating O3 pollution due to NOx emission control in eastern China Sci. Total Environ. 677.

Wesely, M.L., 1989. Parameterization of surface resistances to gaseous dry deposition in regional-scale numerical-models Atmos. Environ. 23, 1293–1304.

Xu L et al 2015 Interannual to decadal climate variability of sea salt aerosols in the coupled climate model CESM1.0 Journal of Geophysical Research: Atmospheres 120.

Xue, L.K., et al., 2014. Ground-level ozone in four Chinese cities: precursors, regional transport and heterogeneous processes Atmos. Chem. Phys. 14, 13175–13188.

Yang, Y., Liao, H., Li, J., 2014. Impacts of the East Asian summer monsoon on interannual variations of summertime surface-layer ozone concentrations over China Atmos. Chem. Phys. 14, 6867–6879.

Yang Y, Liao H and Lou S 2016a Increase in winter haze over eastern China in recent decades: Roles of variations in meteorological parameters and anthropogenic emissions J. Geophys. Res.-Atmos. 121 13050–65.

Yang Y et al 2016b Impacts of ENSO events on cloud radiative effects in preindustrial conditions: Changes in cloud fraction and their dependence on interactive aerosol emissions and concentrations Journal of Geophysical Research: Atmospheres 121 6321–35.

Young, P., et al., 2018. Tropospheric Ozone Assessment Report: Assessment of global-scale model performance for global and regional ozone distributions, variability, and trends Elem Sci Anth 6.

Yue X, Unger N, Harper K, Xia X G, Liao H, Zhu T, Xiao J F, Feng Z Z and Li J 2017 Ozone and haze pollution weakens net primary productivity in China Atmospheric Chemistry and Physics 17 6073–89.

Zhang, H.L., Wang, Y.G., Hu, J.L., Ying, Q., Hu, X.M., 2015. Relationships between meteorological parameters and criteria air pollutants in three megacities in China Environ. Res. 140, 242–254.

Zhang J W, An J L, Qu Y, Liu X G and Chen Y 2019 Impacts of potential HONO sources on the concentrations of oxidants and secondary organic aerosols in the Beijing-Tianjin-Hebei region of China Sci. Total Environ. 647 836–52.

Zheng, B., et al., 2018. Trends in China's anthropogenic emissions since 2010 as the consequence of clean air actions. Atmos. Chem. Phys. 18, 14095–14111.